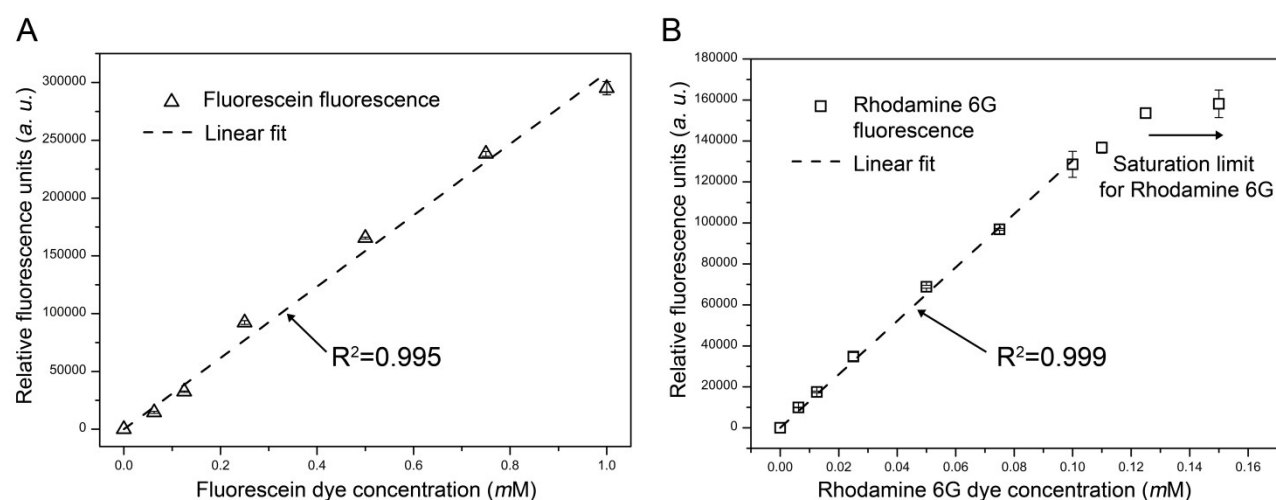


## Supplementary Information

**Supplementary movie 1:** Demonstration of dynamic localization of the stagnation point in response to flow factor adjustment.

**Supplementary movie 2:** Demonstration of dynamic localization of combinational gradients using different concentrations of fluorescein reporter dye. Following a linear relationship to the flow factor, the combinational gradient location can be easily predicted along the *y*-axis shown in Figure 2.



**Fig. S1** Calibration of fluorescence intensity with respect to dye concentration. (A) Fluorescein dye emission intensity was measured at a wavelength of 520nm while (B) Rhodamine 6G dye emission intensity was measured at a wavelength of 580nm. The linear response of fluorescence emitted to actual known dye concentrations indicates that emission intensities derived from concentration gradient images could be directly correlated to actual dye concentrations.

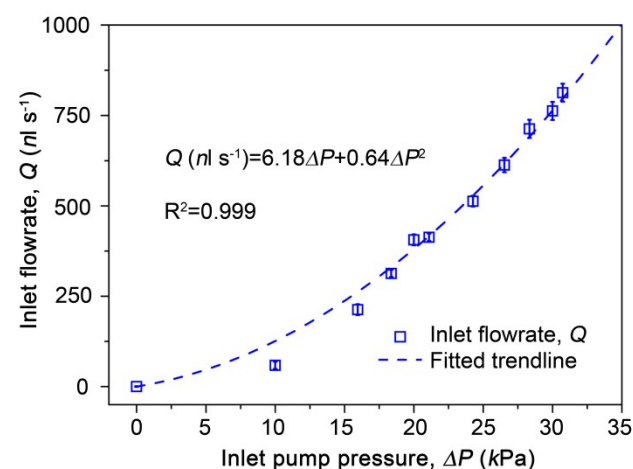


**Fig. S2** Calibration between pump pressure,  $\Delta P$ , and resultant flow rate,  $Q$ , within the MCS device.

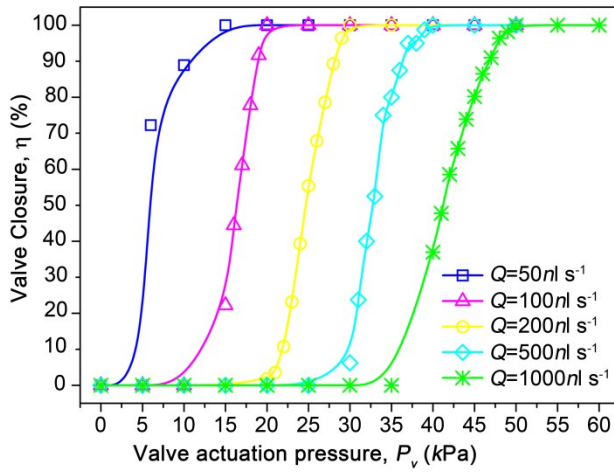


**Fig. S3** Calibration of valving efficiency with respect to valve actuation pressure ( $P_v$ ) across the flow rate range of  $100 \text{ nl s}^{-1}$  to  $1000 \text{ nl s}^{-1}$ . The valving efficiency,  $\eta$  is calculated from the flow rate ratio at different

$$\eta = \frac{Q_{P_v=0} - Q_{P_v}}{Q_{P_v=0}} \times 100\%$$

valve actuation pressures such that

. The valve closure is a function of the inlet flow

rate,  $Q$ , which exerts fluidic back pressure onto the valve membrane during valving operations.

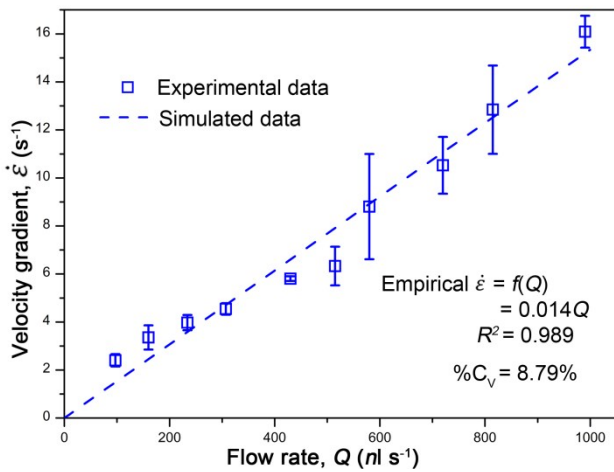


**Fig. S4** Response of velocity gradient,  $\dot{\epsilon}$ , with respect to flow rate,  $Q$ .  $\% C_v$  indicates the  $\%$  variation between the empirical results and the simulated results. Linear relationship indicates Newtonian fluid flow and shows that the velocity gradient can be directly and predictably controlled by flow rate.

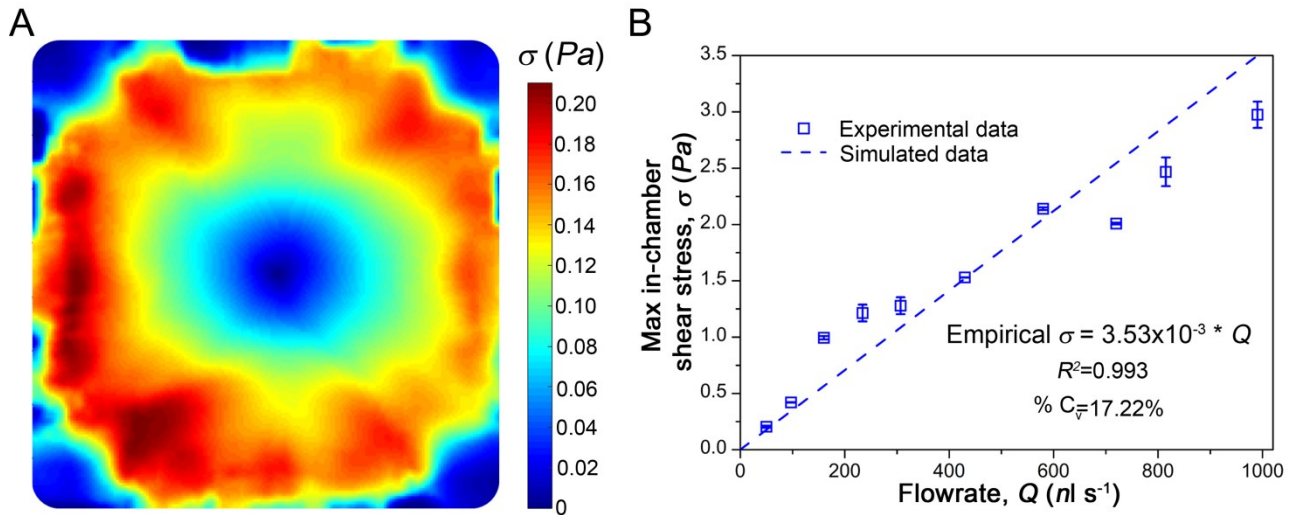


**Fig. S5 (A)** 2D Mapping of flow shear stress based on experimentally measured PIV data (at  $Q=50\text{ml s}^{-1}$ ). Data shows that flow shear stress approaches zero towards the stagnation point at the chamber centre. **(B)** Empirical relationship between the maximum in-chamber shear stress,  $\sigma$ , and the inlets' flow rate,  $Q$ .  $\% C_v$  indicates the  $\%$  variation between the empirical results and the simulated results. The maximum shear stress within the chamber,  $\sigma$ , occurs at the peripheral of the stagnation point and can be predicted based on inlet flow rate.